Role of low-lying resonances for the math xmlns="http://www.w3.org/1998/Math/MathML">mrow>mmultiscripts>mi>Be/mi>mprescripts>/mprescripts>none>/none>mn>10/mn>/mmultiscripts>mo>(/mo>mi>p/mi>mo>,/mo>mi>α/mi>mo>)/mo>mmultiscripts>mi>Li/mi>mprescripts>/mprescripts>none>/none>mn>7/mn>/mmultiscripts>/mrow>/math> reaction rate and implications for the formation of the Solar System

A. Sieverding, J. S. Randhawa, D. Zetterberg, R. J. deBoer, T. Ahn, R. Mancino, G. Martínez-Pinedo, and W. R. Hix

Phys. Rev. C **106**, 015803 — Published 12 July 2022

DOI: 10.1103/PhysRevC.106.015803

The role of low-lying resonances for the ^{10}Be$(p,\alpha)^7$Li reaction rate and implications for the formation of the Solar System

A. Sieverding,[1,*] J. S. Randhawa,[2] D. Zetterberg,[1,3] R. J. deBoer,[2] T. Ahn,[2] R. Mancino,[4,5] G. Martínez-Pinedo,[5,4] and W. R. Hix[1,3]

[1] *Physics Division, Oak Ridge National Laboratory, P.O. Box 2008, Oak Ridge, TN 37831-6354, USA*
[2] *Department of Physics and The Joint Institute for Nuclear Astrophysics, University of Notre Dame, Notre Dame, Indiana 46556 USA*
[3] *Department of Physics and Astronomy, University of Tennessee, Knoxville, TN 37996-1200, USA*
[4] *Institut für Kernphysik (Theoriezentrum), Fachbereich Physik, Technische Universität Darmstadt, Schlossgartenstraße 2, 64298 Darmstadt, Germany*
[5] *GSI Helmholtzzentrum für Schwerionenforschung, Planckstraße 1, 64291 Darmstadt, Germany*

(Dated: June 14, 2022)

Evidence for the presence of short-lived radioactive isotopes when the Solar System formed is preserved in meteorites, providing insights into the conditions at the birth of our Sun. A low-mass core-collapse supernova had been postulated as a candidate for the origin of ^{10}Be, reinforcing the idea that a supernova triggered the formation of the Solar System. We present a detailed study of the production of ^{10}Be by the ν process in supernovae, which is very sensitive to the reaction rate of the major destruction channel, ^{10}Be$(p,\alpha)^7$Li. With data from recent nuclear experiments that show the presence of a resonant state in ^{11}B at $\approx$ 193 keV, we derive new values for the ^{10}Be$(p,\alpha)^7$Li reaction rate which are significantly higher than previous estimates. We show that, with the new ^{10}Be$(p,\alpha)^7$Li reaction rate, a low mass CCSN is unlikely to produce enough ^{10}Be to explain the observed ^{10}Be/^{9}Be ratio in meteorites, even for a wide range of neutrino spectra considered in our models.

I. BACKGROUND

The presence of now-extinct, short-lived ($T_{1/2}$ < 10 Myr) radioactive nuclei (SLRs) in the early Solar System (ESS) has been revealed by systematic anomalies in the abundances of their stable daughter isotopes [1, 2] in meteorites. Since their lifetimes are shorter than the timescales on which the composition of the interstellar medium homogenizes, these radioactive isotopes must have been injected into the Solar System by a nearby nucleosynthesis event or they must have been produced in-situ. Precisely determined abundance ratios of SLRs, thus, provide a very powerful tool to understand the birth environment of our Sun[3]. The requirement to consistently explain all the observed values, however, challenges theoretical models and enrichment scenarios and there is an ongoing debate about the sources of individual isotopes (see [4] for a recent review).

Recent research has added evidence to the idea that core-collapse supernovae (CCSNe) trigger star formation [5–7], making such events prime candidates for the origin of SLRs, as already suggested more than 40 years ago by Cameron and Truran [8]. The isotope ^{10}Be with a half-life of $T_{1/2} = 1.4\,$Myr [9] has mostly been studied in the context of non-thermal, in-situ nucleosynthesis due to cosmic rays or high energy particles from the Sun in its early phases. Such processes have been shown to possibly produce enough ^{10}Be to explain the ESS value [10–14], but rely on assumptions about the cosmic ray spectra, the properties of young stellar objects, and mixing in the ESS. However, ^{10}Be is also produced by the ν process in CCSN explosions [15], i.e., by the interactions of high energy neutrinos emitted from the nascent proto neutron star with nuclei in the outer shells of the massive star. The relevant reactions are the neutral-current reaction ^{12}C$(\nu_x,\nu_x' pp)^{10}$Be and the charged-current reaction ^{12}C$(\bar{\nu}_e, e^+ np)^{10}$Be. In these reactions, interactions with high-energy neutrinos from the tail of the distribution populate high-lying states of ^{12}C and ^{12}B that decay by multi-particle emission. These transitions are usually dominated by the giant resonances and the total cross-section is constrained by sum rules [16], making it relatively insensitive to the details of the nuclear structure. The neutrino spectra from the CCSN are, however, a major uncertainty for the production channel.

Banerjee *et al.* [17] have pointed out that a low-mass CCSN is particularly favorable as source for SLRs in the ESS because the yields of O, Mg, Si, Ca, Fe, and Ni increase steeply with the progenitor mass and would lead to anomalies in the abundances of stable isotopes, which are, however, not observed. They have further demonstrated that such a low-mass CCSN of a 11.8 $M_\odot$progenitor still produces a sufficient yield of ^{10}Be to simultaneously explain the ^{10}Be/^{9}Be, ^{41}Ca/^{40}Ca and ^{107}Pd/^{108}Pd isotopic ratios without creating an overabundance of any of the other SLRs for which abundance ratios have been determined (with the exception of ^{60}Fe if the recent, low values from [18, 19] are assumed). This 11.8 $M_\odot$model is thus a plausible source for ^{10}Be in the ESS.

A major uncertainty for the production of ^{10}Be in CCSNe is the ^{10}Be$(p,\alpha)^7$Li reaction rate. The commonly

* sieverdinga@ornl.gov

used values for the rate from the JINA-REACLIB library [20][21] are estimates from Wagoner [22], based on very little experimental information. Therefore, this rate is quite uncertain but it has been shown to have a significant impact on the ^{10}Be yields [23]. Our study provides a thorough discussion of the sensitivity of ^{10}Be production in CCSNe to the ^{10}Be$(p,\alpha)^7$Li reaction rate, using a range of stellar progenitors and different models of the neutrino spectra. We further identify ^{10}Be$(\alpha,n)^{13}$C as the next important reaction and discuss the role of the neutrino-induced reaction^{10}Be$(\nu_e,e^-)^{10}$B. Using the results of recent experiments that elucidate the lowest nuclear levels of the compound nucleus ^{11}B, we derive an updated nuclear reaction rate for ^{10}Be$(p,\alpha)^7$Li that is significantly higher than the rate commonly used in previous calculations. For the most plausible CCSN model, we show that the new rate reduces the ^{10}Be yield significantly, making it insufficient to explain the ^{10}Be/^{9}Be ratio in the ESS within the uncertainties of the reaction rate and CCSN neutrino emission.

This article is organized as follows: First, in Section II we briefly describe the supernova models and reaction network. In Section III we first describe the general processes relevant for the nucleosynthesis of ^{10}Be and discuss the sensitivity to the ^{10}Be$(p,\alpha)^7$Li rate, as well as the role of the ^{10}Be$(\alpha,n)^{13}$C and ^{10}Be$(\nu_e,e^-)^{10}$B reactions. In Section IV we derive the new ^{10}Be$(p,\alpha)^7$Li reaction rate and discuss the impact on the yields and implications for the ESS in Section V. Finally we conclude in Section VI.

II. SUPERNOVA MODEL

In the following we briefly describe the supernova models and nuclear reaction network used for this study.

To include the dependence on the stellar progenitor model, we use four CCSN and progenitor models that have been studied in Ref. [24], covering stars with zero-age-main-sequence masses of 13 $M_\odot$, 15 $M_\odot$, 20 $M_\odot$ and 25 $M_\odot$ and an initial composition of solar metallicity [25]. Stellar evolution and the explosions have been calculated assuming spherical symmetry with the Kepler hydrodynamics and stellar evolution code [26, 27]. The explosions are driven by a parameterized piston tuned to yield explosion energies $E_{\mathrm{expl}} \approx 1.2\times 10^{51}$ erg, defined as the kinetic energy of the ejecta at infinity.

The models do not track the neutrino emission and we thus use the parameterization from Ref. [15] for the neutrino luminosity and assume the spectra to be constant. For the local neutrino flux at time t and radius $r(t)$ we assume

$$\Phi_\nu(t) = \frac{L_0}{4\pi\, r(t)^2} e^{-t/\tau_\nu} \tag{1}$$

with a timescale of $\tau_\nu = 3\,$s and the luminosity L_0 adjusted to obtain a total energy of 3×10^{53} erg distributed equally among the six neutrino species. The spectra are assumed to be Fermi-Dirac distributions with chemical potential $\mu_\nu = 0$ and characterized with a constant spectral temperature T_ν, related to the average neutrino energy as $\langle E_\nu\rangle \approx 3.15\times T_\nu$. Since the neutrino spectra are a major uncertainty for the production of ^{10}Be we explore two cases that generously cover the range of typical neutrino energies found in current simulations (e.g. [28–30]):

- High E_ν, with $T_{\nu_e} = 4\,$MeV, $T_{\bar{\nu}_e} = 5\,$MeV, $T_{\nu_x} = T_{\bar{\nu}_x} = 6\,$MeV
- Low E_ν, with $T_{\nu_e} = 2.8\,$MeV, $T_{\bar{\nu}_e} = T_{\nu_x} = T_{\bar{\nu}_x} = 4\,$MeV,

where ν_x $(\bar{\nu}_x)$ represent μ and τ neutrinos (antineutrinos).

In practice, the reaction network uses normalized, spectrum-averaged cross sections $\langle\sigma_\nu\rangle$ tabulated as a function of T_ν that are calculated from the energy-dependent cross section $\sigma_\nu(E_\nu)$ as:

$$\langle\sigma_\nu\rangle(T_\nu) = \int_0^\infty \sigma_\nu(E_\nu) f_\nu(E_\nu, T_\nu) dE_\nu, \tag{2}$$

with the normalized distribution function

$$f_\nu(E_\nu, T_\nu) = \frac{N}{T_\nu^3} \frac{E_\nu^2}{1+\exp\left[\mathrm{E_\nu/T_\nu}\right]}, \tag{3}$$

where $N = 2/(3\zeta(3)) \approx 0.55$.

In this study we also include the 11.8 $M_\odot$ progenitor model from Ref. [17] that has been used as the basis for a 3D CCSN simulation [31]. For this progenitor we use a 1D explosion model from Ref. [23], which has been tuned to give a much lower explosion energy of 0.2×10^{51} erg that is consistent with the 3D simulation. We combine this model with the parameterized neutrino exposure described above and additionally include the neutrino emission from the simulation. Note that we do not apply the corrections of Ref. [23], which decrease $\langle E_{\bar{\nu}_e}\rangle$. The average neutrino energies predicted by the simulation are between the parameterized high E_ν and low E_ν cases and evolve with time. The simulation only covers the first 1.3 s after core bounce and we extrapolate the neutrino luminosities as in [23] with an exponential decrease with $\tau_\nu = 2\,$s, and a linear decrease of the neutrino energies, reaching zero at 10 s after bounce.

The explosion trajectories are post-processed with the open-source reaction network code XNet[32], including about 2000 nuclear species, nuclear reactions from the JINA-REACLIB database [20] and most neutrino-nucleus reactions as in Ref. [24]. The neutrino reactions on ^{12}C, which are especially important for the production of ^{10}Be are taken from shell-model calculations of Ref. [33].

^{10}Be is produced by neutrino irradiation of ^{12}C, mainly via the neutral current reaction ^{12}C$(\nu_x,\nu_x' pp)^{10}$Be and the charged-current reaction ^{12}C$(\bar{\nu}_e, e^+ np)^{10}$Be. The

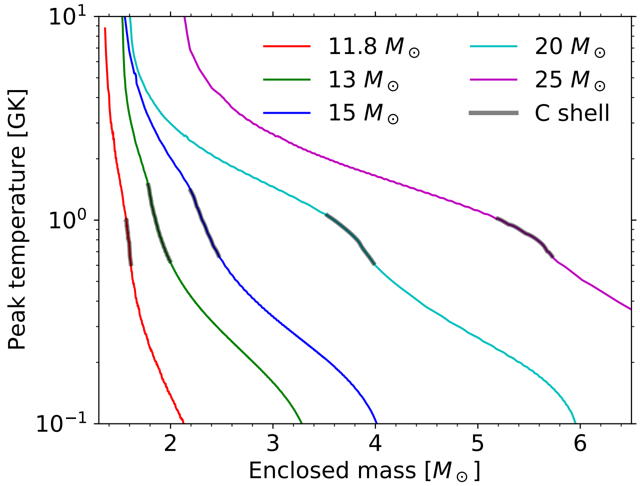

FIG. 1. Peak temperature profiles for the supernova models used here. The C shell, where the production of ^{10}Be occurs, is highlighted in gray. The peak temperature in the C shell ranges from 0.6 to 1.5 GK.

charged current contribution makes the production sensitive to effects of neutrino flavor conversions [23, 33], which transform high energy $\bar{\nu}_x$ into $\bar{\nu}_e$, increasing the contribution of the charged-current channel. Similar effects have been discussed previously in the context of the CCSN ν process [34–36]. Therefore, in Section V we also consider a complete swap of $\bar{\nu}_e \leftrightarrow \bar{\nu}_x$ to estimate the maximal effect of flavor transformations.

The current version of the JINA-REACLIB library does not include a reaction rate for ^{10}Be$(p,n)^{10}$B but Kusakabe *et al.* [34] have calculated the rate with the statistical model and they do not find a noticeable impact on the nucleosynthesis yields. Their values for the reaction rate are more than an order of magnitude lower than the ^{10}Be$(p,\alpha)^7$Li reaction rate. The data from the direct measurement of ^{10}Be$(p,n)^{10}$B [37] is even lower than the Hauser-Feshbach based statistical model calculations which makes this reaction even less significant for destruction of ^{10}Be and hence we did not consider it in our calculations and we did not consider it in our calculations.

III. PRODUCTION OF ^{10}Be AND SENSITIVITY STUDY

A. Overview

The production of ^{10}Be is dominated by neutrino induced reactions and, therefore, the spectra are a major uncertainty on the side of the astrophysical modelling. We cover this uncertainty by including the low and high E_ν spectra defined above. Nuclear reactions have predominantly a destructive effect on ^{10}Be. To better understand the sensitivity of ^{10}Be yields to the nuclear reaction rates, we illustrate in the following the processes that contribute to the production and destruction of ^{10}Be. As ^{10}Be is produced from ^{12}C via neutrino induced reactions, the initial mass fraction (X) of ^{12}C determines the parts of the CCSN ejecta where ^{10}Be can be produced. For the five CCSN models that we study here, the peak temperature in the C-shell ranges from 0.6 GK to 1.5 GK. This is illustrated in Fig. 1 which shows the peak temperature for all the models with the C shell highlighted as thick gray lines. The peak temperature is very important for the impact of nuclear reactions and in a radiation dominated case it depends only mildly on the explosion energy with $T_{\rm Peak} \propto E_{\rm expl}^{1/4}$. In the following we describe the ^{10}0Be production for our calculations with the 15 $M_\odot$ model in more detail as an example. The qualitative picture is similar for all the progenitor models.

The top panel of Fig. 2 shows the pre-supernova mass fraction profile of ^{12}C as well as ^{20}Ne, ^{16}O and ^{4}He for the 15 $M_\odot$ progenitor model. The O/Ne shell below a mass coordinate of around 2.2 $M_\odot$ has been processed by C-shell burning, leading to a reduced mass fraction of ^{12}C and an increase of ^{20}Ne. The region with $X(^{12}\mathrm{C}) > 0.05$, starting at a mass coordinate around 2.2 $M_\odot$ (corresponding to a radius of 15,000 km) is shown with a gray background and we will refer to this region as the C shell in the following. The bottom of the C shell is depleted in ^{4}He, i.e., $X(^4\mathrm{He}) < 0.01$, and this region is further shaded in dark gray. Above 2.25 $M_\odot$, α particles are leftover and in a narrow region $X(^{12}\mathrm{C}) > X(^{16}\mathrm{O})$. The ^{4}He mass fraction gradually increases toward the He shell. The bottom of the He shell, up to 2.9 $M_\odot$, also contains a low level of ^{12}C.

The final mass fraction of ^{10}Be at 200 s after the explosion is shown in the middle panel of Fig. 2 and it is strongly peaked at the He-free bottom of the C shell. The bottom panel shows the time-integrated net reaction fluxes of the two dominant destruction reactions, ^{10}Be$(p,\alpha)^7$Li and ^{10}Be$(\alpha,n)^{13}$C. The integrated net flux of a reaction $A \rightarrow B$ is defined as

$$\mathcal{F}_{A\rightarrow B} = \int_{t_0}^{t_{\rm stop}} \dot{y}_{A\rightarrow B}(t) + \dot{y}_{B\rightarrow A}(t)\,\mathrm{d}t, \tag{4}$$

where the integral covers the whole duration of the calculation, i.e., 200 s, $\dot{y}_{A\rightarrow B}(t)$ and $\dot{y}_{B\rightarrow A}(t)$ are the change of the abundance of A due to the forward and inverse reactions, respectively, at a given time. The magnitude of the integrated flux of the destructive reactions is larger than the final abundances of ^{10}Be, indicating that only a fraction of the produced abundance survives. Fig. 2 shows that we can distinguish between two regions that are indicated by the light and dark gray regions:

1. The bottom of the C shell, where ^{4}He has been depleted almost completely, dominates the final yield of ^{10}Be and ^{10}Be$(p,\alpha)^7$Li is the most important destructive nuclear reaction.

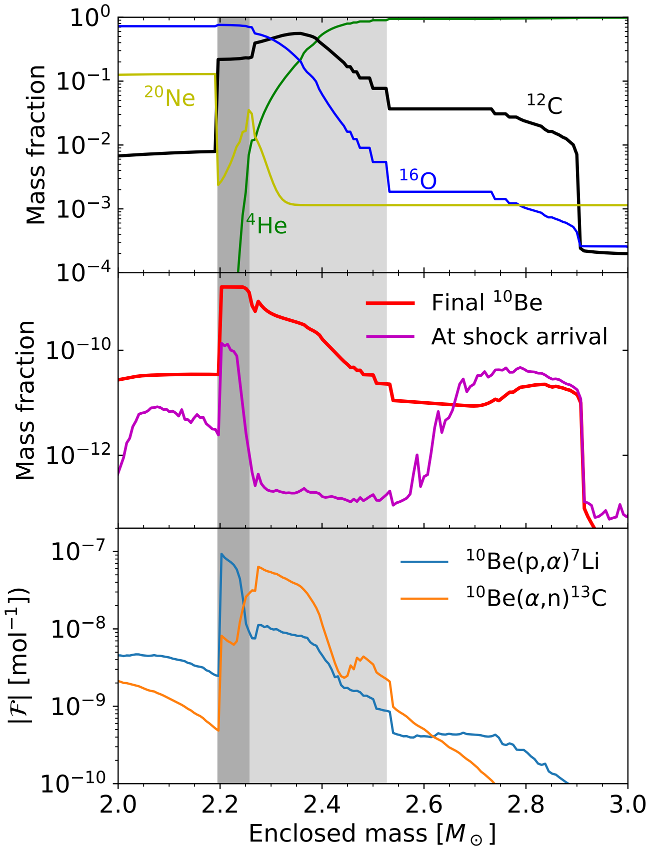

FIG. 2. Mass fraction profile of the 15 $M_\odot$ model. The top panel shows the pre-supernova mass fractions of several important isotopes to indicate the star's compositional layers. The middle panel shows the profiles of the ^{10}Be mass fraction at 200 s (Final) and at the time of shock arrival, i.e., when the peak temperature is reached. Note that this time is different for each location. The bottom panel shows the absolute value of the integrated net reaction fluxes, $\mathcal{F}$, as defined in Eq. (4) due the two most important destructive reactions.

2. In the outer C shell a significant mass fraction of ^{4}He is still present and ^{10}Be$(\alpha,n)^{13}$C is the dominant destructive reaction, limiting the contribution of this region to the production of ^{10}Be.

The ^{10}Be yield is largest at the bottom of the C shell because at higher enclosed mass values, even though $X(^{12}\mathrm{C})$ is higher, ^{4}He becomes more abundant and therefore destroys ^{10}Be via the ^{10}Be$(\alpha,n)^{13}$C reaction. At the bottom of the C shell, free protons need to be released first to inhibit the production of ^{10}Be. In addition to nuclear reactions and photo-disintegration activated by the shock, neutrino-induced reactions, such as the neutral current reaction $^{16}\mathrm{O}(\nu_x,\nu_x' p)^{15}\mathrm{N}$, play an important role as a proton source. In particular at later times, when the temperature is too low for photo-disintegration, neutrino reactions continue to provide protons. The neutrino reactions are also important proton sources in the outer C shell and the bottom of the He shell, where the peak temperatures are low. Before the shock hits, the temperature is relatively low, allowing the neutrino interactions to build up ^{10}Be. When the shock hits, the destruction reactions are most effective while the temperature remains high. Free protons are quickly consumed, suppressing the ^{10}Be$(p,\alpha)^7$Li reaction and allowing the ^{10}Be abundance to recover. Due to neutrino-interactions, the proton abundance also increases again. In cases where the temperature remains high for long enough or when the reaction rate is enhanced, the destructive reaction becomes active again, leading to a decrease of the ^{10}Be mass fraction at late times. This possibility of late-time destruction is important for the impact of an enhanced reaction rate as illustrated in Fig. 4 and is discussed in more detail below. Most of the ^{10}Be yield is only produced after the shock has passed. This is illustrated by the middle panel of Fig. 2, which shows that the ^{10}Be mass fraction at the time when the peak temperature is reached is much smaller than the final mass fraction everywhere in the C shell. At the bottom of the He shell, however, where ^{12}C is also present, the peak temperature is too low for the efficient destruction of the SLR by the SN shock. Here, the final ^{10}Be mass fraction is lower than the mass fraction at the time of shock arrival, illustrating that the (p,α) reaction continues to be active after the shock has passed.

The relative contribution of the bottom of the C shell varies with progenitor mass due to different sizes of the shells, different temperatures and distance from the proto neutron star as well as differences in the initial composition. For the 11.8 $M_\odot$ model about 50 % of the total ^{10}Be yield is provided by the He-free bottom of the C shell. For the 15 $M_\odot$ model the contribution of the bottom of the C shell is almost 70 %.

In the 25 $M_\odot$ model, the O/Ne shell, which is much larger in terms of mass than the C shell, has a ^{12}C mass fraction that is higher by almost an order of magnitude compared to the 15 $M_\odot$ model. Therefore, for the 25 $M_\odot$ model, the O/Ne shell contributes 80% of the ^{10}Be yield. The details of this process are subject to the uncertainties of the astrophysical modeling, including all of the assumptions made in the stellar evolution model as well as the details of the explosion. In addition to the explosion energy that is crucial for setting the temperature, the shock velocity and time evolution of the neutrino emission [38] have an impact on the yields. A full analysis of these uncertainties is beyond the scope of this article, but we cover the uncertainties of the neutrino emission with our low and high E_ν cases and the impact of the progenitor model by exploring a range of stellar masses.

B. Sensitivity to ^{10}Be$(p,\alpha)^7$Li

To explore the sensitivity of the ^{10}Be yield to the ^{10}Be$(p,\alpha)^7$Li rate, we perform post-processing reaction network calculations including a global, i.e., temperature-independent, multiplier $\mathcal{R}$ for this rate. The

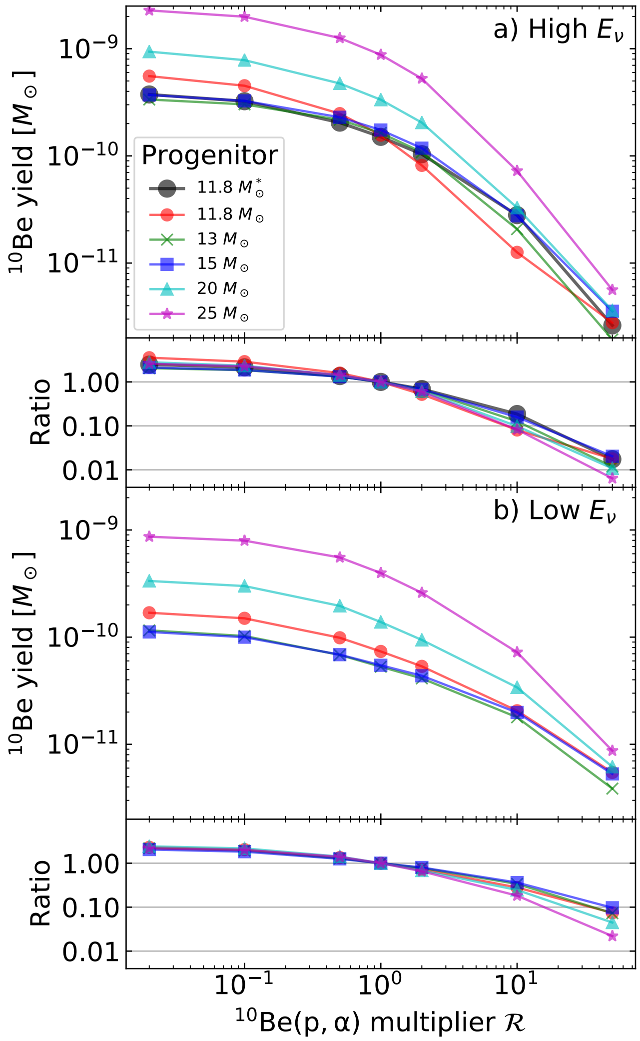

FIG. 3. Impact of the variation of the ^{10}Be(p,α) reaction rate on the ^{10}Be yields and ratio relative to the result with the JINA-REACLIB reaction rate. The upper two panels are for high E_ν and the lower two panels for low E_ν. The results with the neutrino spectra from the 3D simulation of the 11.8 $M_\odot$ model is also included in the upper panel (11.8 $M_\odot$*).

existence of resonances can have a large impact, as we will show in Section V. Therefore, we explore a large range, increasing and decreasing the rate by factors 2, 10 and 50 relative to the JINA-REACLIB value. The inverse reaction, ^{7}Li(α,p), is strongly suppressed due to the negative Q-Value and Coulomb barrier. Furthermore, the mass fraction of ^{7}Li does not exceed 10^{-7}, making it a relatively rare target. Thus, for the conditions relevant here, we assume the reverse reaction to be negligible and keep its rate unchanged for the sensitivity analysis. The effect of the inverse reaction is included in Section V.

Fig. 3 shows the ^{10}Be yield as a function of the reaction rate multiplier for the five stellar models considered here. The top panel shows the results for high E_ν and the bottom panel the results for low E_ν. The neutrino spectra from the 11.8 $M_\odot$simulation are time-dependent, but tend to be in between the high and low energy cases and the results are included in the top panel.

For a suppression of the ^{10}Be$(p,\alpha)^7$Li reaction, i.e., for $\mathcal{R} < 1$, the yields moderately increase. The increase is limited by the ^{10}Be$(\alpha,n)^{13}$C reaction, which eventually becomes dominant. The bottom panel of Fig. 2 shows that the reaction flux through ^{10}Be$(p,\alpha)^7$Li is at most one order of magnitude higher than the flux through ^{10}Be$(\alpha,n)^{13}$C. The latter reaction can thus be expected to become dominant if $\mathcal{R} \lessapprox 0.1$. Accordingly, in Fig. 3 we only see a small increase of the yield from $\mathcal{R} = 0.1$ to $\mathcal{R} = 0.02$.

For the 11.8 $M_\odot$ model with high E_ν, the increase relative to the results with the default reaction rate is largest, reaching a factor of 3.5 for $\mathcal{R} = 0.02$. For all other models, the ratio of the yield relative to the yield with the default reaction rate ranges from a factor of 2.0 to 2.7. Ref. [23] found that turning off the ^{10}Be$(p,\alpha)^7$Li reaction completely increases the yield by a factor 3, which is consistent with the range of values we find here.

An increase of the ^{10}Be$(p,\alpha)^7$Li rate, i.e., $\mathcal{R} > 1$ in Fig. 3, efficiently reduces the yield. As explained above, the ^{10}Be$(p,\alpha)^7$Li reaction is still active after the shock has passed and reduces the peak mass fraction of ^{10}Be. Given a sufficiently high temperature and high rate, the reaction will tend to destroy practically all of the ^{10}Be. For an individual trajectory, an increase of $\mathcal{R}$ reduces the peak ^{10}Be mass fraction that is accumulated after the shock and it also extends the time during which the destruction operates after the production has ceased. This makes the final yield very sensitive to $\mathcal{R}$. Figure 5 illustrates the strong impact of the enhancement of the rate and it also shows that the effect is most pronounced at the bottom of the C shell, where the temperature is highest. For $\mathcal{R} = 10$, only $8-15\,\%$ $(18-35\,\%)$ of the yield with the default rate are left, with high (low) E_ν. In relative terms, the reduction is largest for the 25 $M_\odot$ model because of the large contriution from the O/Ne shell and the higher peak temperature which enhances the reaction.

As $\mathcal{R}$ increases, ^{10}Be is more effectively destroyed at high temperatures, shifting the main production to lower temperatures. Furthermore, the ^{10}Be$(p,\alpha)^7$Li reaction also remains effective at a lower temperature and thus at later times, when protons from thermonuclear reactions are increasingly rare. Both of these effects make the role of neutrino-induced reactions as proton sources more important for larger $\mathcal{R}$. As a consequence, the yields decrease faster with $\mathcal{R}$ for high E_ν than for low E_ν, as shown by the ratios in Figure 3.

The role of neutrinos as a proton source also leads to the effect that the ^{10}Be yields with high E_ν become lower than the results with low E_ν for higher values of $\mathcal{R}$, which is visible when comparing the upper and lower panel of Fig. 3. This effect is more clearly illustrated in Fig. 4 which shows the time evolution of the ^{10}Be and proton mass fractions for a zone at 2.32 $M_\odot$ in the 15 $M_\odot$

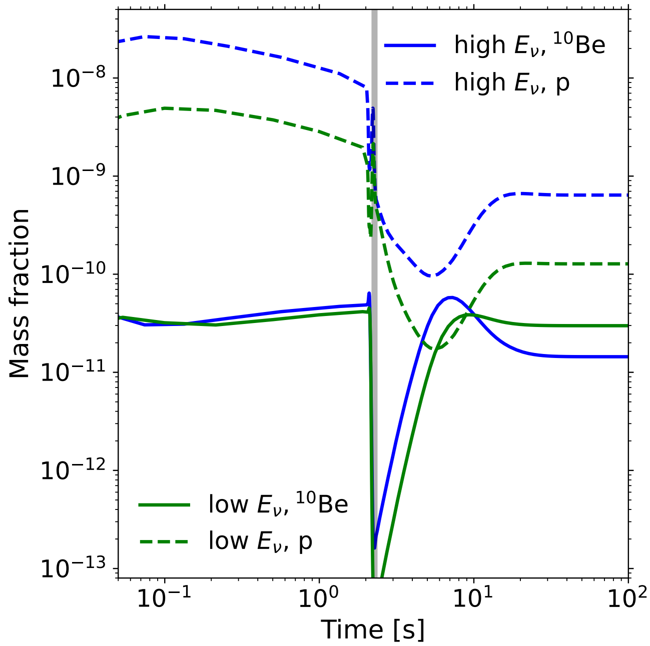

FIG. 4. Time evolution of the mass fractions of free protons and ^{10}Be for the 15 $M_\odot$ model in the outer C shell at mass coordinate of 2.32 $M_\odot$ and with the $^{10}\mathrm{Be}(p,\alpha)^7\mathrm{Li}$ rate enhanced by a factor 50 for low and high E_ν. With high E_ν the proton mass fraction is enhanced by almost factor of 10, leading to a lower final ^{10}Be mass fraction than in the low E_ν case.

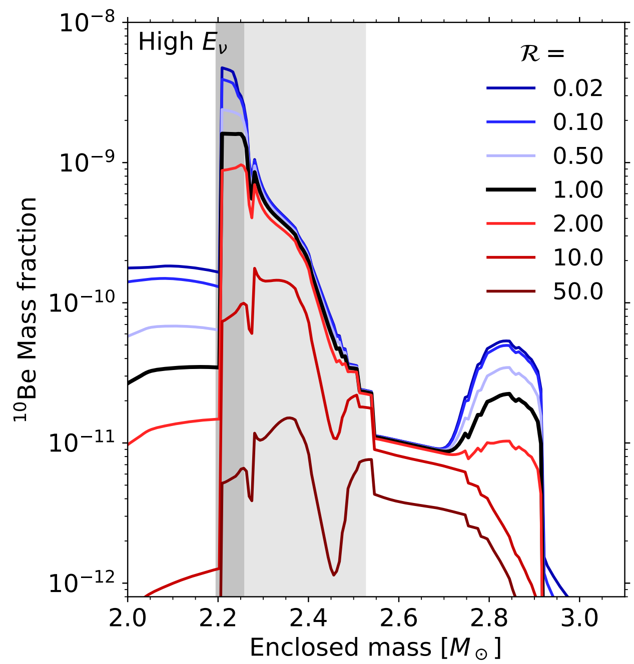

FIG. 5. Mass fraction profile of ^{10}Be for the 15 $M_\odot$model with high E_ν for the range of values of the $^{10}\mathrm{Be}(p,\alpha)^7\mathrm{Li}$reaction rate multiplier $\mathcal{R}$. The contribution of the bottom of the C shell decreases with increasing $\mathcal{R}$.

model for $\mathcal{R} = 50$ comparing the high E_ν and low E_ν cases. The arrival of the SN shock is marked as a gray vertical line when most of the initially produced ^{10}Be is destroyed. The final mass fraction is determined by the production after the shock has passed. With high E_ν the proton mass fraction is significantly higher, allowing the enhanced $^{10}\mathrm{Be}(p,\alpha)^7\mathrm{Li}$ reaction to reduce the ^{10}Be mass fraction even at 10 s, when the temperature has dropped to 0.4 GK. As a result, even though the peak mass fraction of ^{10}Be reached at 6 s is higher for high E_ν, the final mass fraction is higher for low E_ν because of the lower proton abundance. Note that this inversion does not occur with the default $^{10}\mathrm{Be}(p,\alpha)^7\mathrm{Li}$ reaction rate, because the reaction is too slow at low temperatures. For the 15 $M_\odot$ model, this effect becomes only noticeable for $\mathcal{R} = 50$, when the yield is $3.5 \times 10^{-12}\,M_\odot$ for high E_ν and $5.3 \times 10^{-12}\,M_\odot$ with low E_ν.

The effect is more pronounced for the 11.8 $M_\odot$ model because it has a much lower explosion energy and peak temperatures are generally lower, increasing the importance of neutrinos to provide protons. For example, for the 11.8 $M_\odot$ model with $\mathcal{R} = 10$, the high E_ν case actually results in the lowest yield among all models for this value of $\mathcal{R}$, which is $1.3 \times 10^{-11}\,M_\odot$. For comparison, the yield is $2.8 \times 10^{-11}\,M_\odot$ with the neutrino spectra from the simulation and $2.1 \times 10^{-11}\,M_\odot$ with low E_ν. The yield with the neutrino spectra from the simulation is highest, because the neutrino temperatures decrease with time and the luminosities decrease faster, reducing the proton mass fraction at late times. This illustrates the complex interplay between the sensitivity to the reaction rate and the sensitivity to the neutrino spectra in the ν process.

In Section III A we have shown that the He-free bottom of the C shell dominates the yields for the JINA-REACLIB reaction rate. Since the $^{10}\mathrm{Be}(p,\alpha)^7\mathrm{Li}$ reaction is the main destructive channel in that region, its relative contribution to the total yield decreases first as $\mathcal{R}$ increases. This is illustrated in Fig. 5 for the 15 $M_\odot$model and shows that the He-rich, outer C shell already becomes the dominant production region for $\mathcal{R} = 10$. For different progenitors the differences in the relative contributions of the different shells and the different temperatures in the respective regions determine the details of the behaviour of the yield as a function of $\mathcal{R}$. The overall trend, however, is very similar for all the models, with a slight increase of the yield for $\mathcal{R} < 1$ and a much steeper decrease for $\mathcal{R} > 1$.

C. Sensitivity to $^{10}\mathrm{Be}(\alpha,n)^{13}\mathrm{C}$

The reaction $^{10}\mathrm{Be}(\alpha,n)^{13}\mathrm{C}$ has already been mentioned in Ref. [33] as most important destructive reaction using, however, an older and much higher value of the rate. With the currently recommended rate in the JINA-REACLIB library we find it to be the second most important destruction channel for ^{10}Be after ^{10}Be$(p,\alpha)^7$Li. Fig. 2 shows that ^{10}Be$(\alpha,n)^{13}$C is generally dominant in the outer regions, where α particles are leftover from incomplete He-burning. The reaction limits the contribution from this region to the total ^{10}Be yield. The default reaction rate in the JINA-REACLIB database is up to a factor 100 lower than the values in STARLIB [39]. Due to this large difference, we explore a global variation of the reaction rate from the JINA-REACLIB database by factors 10 and 50 up and down, while keeping the ^{10}Be$(p,\alpha)^7$Li reaction rate from the JINA-REACLIB library. Increasing the ^{10}Be$(\alpha,n)^{13}$C reaction rate by a factor 50 (10) for the 15 $M_\odot$ model with high E_ν reduces the yield from 1.7×10^{-10} $M_\odot$ by a factor 1.9 (1.4) to 0.9×10^{-10} $M_\odot$ (1.2×10^{-10} $M_\odot$). Suppressing the reaction rate by a factor 50 (10), on the other hand yields an increase by a factor 1.6 (1.4), to 2.7×10^{-10} $M_\odot$ (2.3×10^{-10} $M_\odot$) of ^{10}Be. Based on this, we estimate the overall uncertainty due of the ^{10}Be yields due to this reaction rate to be up to a factor of 2. Thus, for a full understanding of the ^{10}Be production in CC-SNe, a re-evaluation of experimental constraints on the cross section for ^{10}Be$(\alpha,n)^{13}$C or a direct measurement is highly desirable.

D. Sensitivity to ^{10}Be$(\nu_e,e^-)^{10}$B

The reaction ^{10}Be$(\nu_e,e^-)^{10}$B may contribute to the destruction of ^{10}Be [23]. An estimate of the cross section was previously provided in the global compilation of neutrino cross sections of Ref. [24]. Here, we improve it by combining shell-model calculations and experimental data. From the beta-decay data of the mirror nucleus of ^{10}Be, ^{10}C, we expect that ν_e absorption on ^{10}Be will have a large Gamow-Teller (GT) contribution to the 1^+ state at 718 keV in ^{10}B, $\log ft = 3.0426(7)$, $B(GT) = 5.573(9)$ [40]. In addition, we expect a Fermi contribution to the 0^+ state at 1.740 keV. To determine whether other states may further enhance the cross section, we have performed a shell model calculation with the code NATHAN [41] employing the Cohen-Kurath interaction [42]. The theoretical GT matrix elements have been reduced by a quenching factor $q = 0.82$ [43]. We find that the GT transition at 718 keVdominates the cross-section at the relevant neutrino energies. No noticeable reduction of the ^{10}Be yield is found, even assuming $T_{\nu_e} = 6\,$MeV, because the abundance of ^{10}Be is never large enough to allow for a noticeable number of interactions. For completeness, we provide the values of the spectrum averaged cross-sections in Table I.

IV. NEW ^{10}Be$(p,\alpha)^7$Li REACTION RATE

The ^{10}Be$(p,\alpha)^7$Li reaction proceeds through the ^{11}B compound nucleus where states above the proton emission threshold play an important role. Current estimates of the ^{10}Be$(p,\alpha)^7$Li reaction rate are based on estimates by Wagoner [22] and it is the default reaction rate in JINA-REACLIB. We refer to this rate as the REACLIB rate hereafter. While the REACLIB rate was based on a constant S-factor approximation, this reaction is expected to be dominated by isolated resonances in the Gamow window. In recent years, states near the proton threshold in ^{11}B have gained significant attention as they can explain the puzzling β^-p$^+$ decay in ^{11}Be. A recent experiment, which directly measured the protons and their energy distribution, shows that the decay proceeds sequentially though a narrow reso-

TABLE I. Spectrum averaged cross-section for ν_e absorption on ^{10}Be as defined in Eq. (2).

T_ν (MeV)	2.8	3.5	4.0	5.0	6.4	8.0	10.0
$\langle\sigma_{\nu_e}\rangle(10^{-42}\mathrm{cm}^2)$	14.6	22.8	29.7	46.2	73.2	105.3	141.3

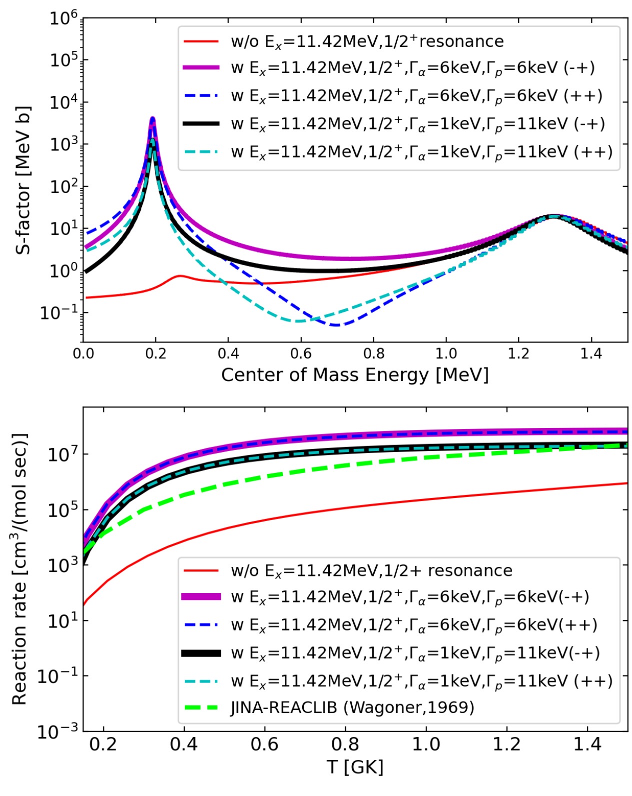

FIG. 6. R-matrix calculations to assess the impact of the 193 keV $1/2^+$ resonance on the ^{10}Be(p,α) reaction cross section. The upper panel shows the S-factor and the lower panel the reaction rate as a function of temperature. Results without the 193 keV $1/2^+$ resonance are shown (red line) as well several results assuming different resonance widths and assumptions about the interference with the $3/2^+$ resonance (see text). For comparison, the rate from [22] is also shown (green dashed line). The result with $\Gamma_p = 6$ keV, $\Gamma_\alpha = 6$ keV, (+-) is the new recommended rate.

nance [$E = 11425(20)$ keV, $\Gamma = 12(5)$ keV, $J^\pi = (1/2^+, 3/2^+)$] in ^{11}B [44]. Preceeding this experiment, it was shown that Shell Model Embedded in the Continuum (SMEC) calculations strongly favor the J^π=1/2$^+$ assignment over 3/2$^+$ [45]. This 1/2$^+$ resonance at ≈193 keV (^{11}B $S(p) = 11228$ keV), proves to be most crucial for the ^{10}Be$(p,\alpha)^7$Li reaction rate as it is well within the Gamow window and provides the dominant contribution to ^{10}Be$(p,\alpha)^7$Li reaction rate throughout, as discussed in detail below.

In this work, we have re-evaluated the ^{10}Be$(p,\alpha)^7$Li reaction rate using the R-matrix approach using the code `AZURE2` [46, 47]. For the R-matrix calculations, other than the known energy levels in ^{11}B above the proton emission threshold, we have included the recently observed 11.425 MeV state (193 keV 1/2$^+$ resonance, discussed above), which is one of the main highlights of this work. In addition, we have also included a 3/2$^+$ state at 11.490 MeV, predicted by Refsgaard *et al.* [48] to explain the β-delayed α-spectrum from ^{11}Be and later discussed by Okołowicz *et al.* [45].
All energy levels considered for the current R-matrix calculations and corresponding parameters are shown in Table II. Energies of the states and partial widths are adopted from the NNDC database wherever possible [49]. In the absence of data, reduced widths are adopted as ≈$0.01\gamma_W^2$, where γ_W^2 is the Wigner limit [50]. The results of the R-matrix calculations are shown in Fig. 6 where the upper panel shows the astrophysical S-factor as a function of center-of-mass energy and the lower panel shows the reaction rate versus temperature. Fig. 6 (upper panel) shows the S-factor with and without the 193 keV resonance contribution. The cross section without the 193 keV resonance (red line) is dominated in the Gamow window (90 keV-410 keV) by the low energy tail of the broader, higher lying 1/2$^+$ resonance ($E_x = 12.55$ MeV). When the 193 keV 1/2$^+$ resonance is included (magenta and blue lines), the cross section in the Gamow window is completely dominated by this resonance and is several orders of magnitude higher. Moreover, the effect of a 3/2$^+$ state at 11.490 MeV, which is included in the calculations, is negligible for the overall cross-section. We also considered the interference between the 1/2$^+$ states where (-+) and (++) represents the different relative signs of channels and found that this did not have a significant effect on the reaction rate.

Fig. 6 (lower panel) shows the comparison of new reaction rates, with and without the 193 keV 1/2$^+$ state, as well as to th REACLIB rate [20] (green dotted line) in the temperature range relevant for the production of ^{10}Be as indicated in Fig. 1. A maximum predicted rate (Magenta line) is obtained when the 193 keV 1/2$^+$ resonance is included with its maximum strength (Γ_p = 6 keV, Γ_α = 6 keV). Here, it is worth mentioning that from the recent proton resonant scattering ^{10}Be(p,p), and ^{10}B(d,p) experiments both confirms the presence of the 193 keV 1/2$^+$ resonance, proton partial width of $\Gamma_p = 6$ keV [51, 52]. Therefore, these widths are based on recent experimental results and we refer to this rate as the new recommended rate in the following. To assess the sensitivity of the reaction rate to the partial widths of the resonance at 193 keV, we also considered another extreme. The lower predicted rate (black line), which includes the 1/2$^+$ resonance but with a smaller strength resulting from $\Gamma_p = 11$ keV and $\Gamma_\alpha = 1$ keV is an extreme case scenario to explore if such a large change in the partial widths could result in a sufficient yield of ^{10}Be. This rate hereafter is referred as lower rate. The lower rate and the recommended rate are factors of ∼200 to ∼1000 higher compared to the rate derived without the 193 keV 1/2$^+$ resonance, respectively. This shows that the 193 keV resonance has a large impact on the ^{10}Be$(p,\alpha)^7$Li reaction rate in the Gamow window relevant for CCSNe. Compared to the REACLIB rate, our lower and recommended rate are higher by a factor of ≈6 and ≈20 in the Gamow window.

TABLE II. Levels included in the R-matrix calculations.

Energy (MeV)	J^π	partial widths (keV)
11.272	9/2$^+$	Γ_p=10^{-15}, Γ_α = 110
11.425	1/2$^+$	Γ_p=6,11, Γ_α=6,1
11.490	3/2$^+$	Γ_p=10^{-4} Γ_α=93
11.600	5/2$^+$	Γ_p=10^{-5}, Γ_α=90, Γ_n=90
11.893	5/2$^-$	Γ_p=10^{-4}, Γ_α=100, Γ_n=94
12.040	7/2$^+$	Γ_p=10^{-3}, Γ_α=500, Γ_n=500
12.550	1/2$^+$	Γ_p=100, Γ_α=105

For the nucleosynthesis calculations in Section V, we consider both, the recommended and lower rate to estimate the impact of the remaining uncertainty in ^{10}Be$(p,\alpha)^7$Li reaction rate.

V. IMPACT OF THE NEW ^{10}Be$(p,\alpha)^7$Li REACTION RATE

A. Impact on Supernova Yields

The new ^{10}Be$(p,\alpha)^7$Li reaction rate is based on the updated nuclear data as described in Section IV. Our recommended rate is factor of ∼20 higher compared to the REACLIB rate. The reaction network calculations use the parameterization given in Appendix A and include the rate for the inverse reaction,^{7}Li$(\alpha,p)^{10}$Be, using detailed balance. The inverse reaction is only noticeable with high E_ν and results in an increase in the yield by less than 20%.

Figure 7 summarizes the range of ^{10}Be yields obtained with the new reaction rates for the five progenitor models and compares the high and low E_ν cases. The results with the REACLIB rate are shown for comparison. From Figure 7, the ^{10}Be yield trend shows that the yield increases with increasing progenitor mass from 15 $M_\odot$to 25 $M_\odot$because the amount of material in the C shell increases. As noted by [17], however, the yields for the

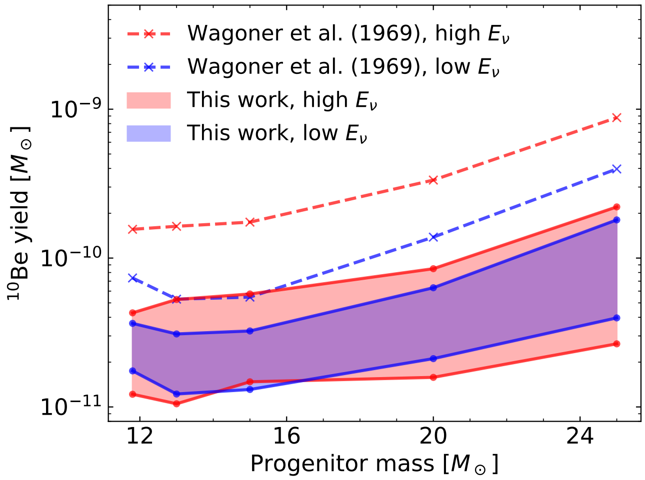

FIG. 7. ^{10}Be yields for the models studied with high and low E_ν. The red and blue shaded bands indicate the range of results between the lower and recommended rate from Section IV. For comparison, the dashed lines indicate the results with the JINA-REACLIB rate from [22] from models with the corresponding neutrino spectra. Note that we assumed and explosion energy of 0.2×10^{51} erg for the 11.8 $M_\odot$and 1.2×10^{51} erg for all other models.

progenitors from 11.8 $M_\odot$to 15 $M_\odot$are relatively similar. For high E_ν the yield even decreases slightly from 11.8 $M_\odot$to 13 $M_\odot$. This is because the 11.8 $M_\odot$model assumes a lower explosion energy, leading to lower peak temperatures that favor the survival of ^{10}Be. The spread in the ^{10}Be yields with the lower and recommended rate for a given E_ν model is indicated by the colored bands and represents the impact of current uncertainty in the ^{10}Be$(p,\alpha)^7$Li reaction rate. This band is slightly narrower with low E_ν compared to high E_ν due to the role of neutrino-induced reactions as proton sources. In general, lower explosion energies lead to lower peak temperatures that favor the survival of ^{10}Be. For models 13-25 $M_\odot$a typical explosion energy of 1.2×10^{51} erg was assumed. Significantly lower explosion energies may enhance the ^{10}Be yield in nature. Current models and observation, however indicate explosion energies in the rang of $(0.8-1.6)\times10^{51}$ erg for stars in this mass range [53] and due to the weak dependence of the temperature on the energy, this corresponds to a relatively small variation of around 10 % in $T_{\rm peak}$. The explosion energy of the 11.8 $M_\odot$model is furthermore already taken to be very low as indicated by a state-of-the-art 3D simulation with this progenitor and it is consistent with the observation of low ^{56}Ni yields of such explosions [54–56]. Compared to the results with the REACLIB rate, using the new recommended reaction rate and high E_ν (low E_ν), the ^{10}Be yield is decreased by factors of ∼13-33 (4-10). This significant change shows that the ^{10}Be$(p,\alpha)^7$Li reaction is indeed a major destruction channel of ^{10}Be in CCSNe and challenges the scenario in which ^{10}Be was injected by a nearby Supernova into the ESS.

TABLE III. ^{10}Be yields for the lower and recommended value of the ^{10}Be$(p,\alpha)^7$Li reaction rate and different models for the neutrino spectra. Yields are given in units of $10^{-10}\,M_\odot$. Scenarios marked with "$(\bar\nu_x \leftrightarrow \bar\nu_e)$" assume a complete swap of the $\bar\nu_x$ and $\bar\nu_e$ spectra by flavor transformations.

Model	Neutrino Spectrum	lower rate	Recommended rate
1	Low E_ν	0.36	0.18
2	Simulation	0.65	0.20
3	High E_ν	0.43	0.12
4	Simulation $(\bar\nu_x \leftrightarrow \bar\nu_e)$	0.80	0.24
5	High E_ν $(\bar\nu_x \leftrightarrow \bar\nu_e)$	1.23	0.34

B. Implications for Early Solar System

A major problem in reconciling theoretical CCSN nucleosynthesis yields with the abundances of SLRs in the ESS is the absence of anomalies in the isotopic composition of common stable isotopes. This excludes most CCSNe [57], except for those from low-mass progenitors with low explosion energies as the origin of the SLRs [17]. Banerjee *et al.* [17] have further demonstrated that a 11.8 $M_\odot$progenitor produces a sufficient yield of ^{10}Be to simultaneously explain the ^{10}Be/^{9}Be, ^{41}Ca/^{40}Ca and ^{107}Pd/^{108}Pd inferred isotopic ratios, identifying this model as a favorable candidate to explain the ESS SLR abundances. Therefore, we focus in the following on this model and show that, with the new reaction rate discussed above, the yield of the 11.8 $M_\odot$model is insufficient to explain the ^{10}Be/^{9}Be ESS ratio in the scenario proposed by Banerjee *et al.* [17]. To estimate the required yields, the ESS ratio between the number of nuclei of the SLR, N_{SLR} and the number of nuclei of the reference isotope N_I, implied by a CCSN yield Y_{SLR} of a radioactive isotope with mass number A_{SLR} is estimated as

$$\left(\frac{N_{SLR}}{N_I}\right)_{\rm ESS} = \frac{f\,Y_{SLR}/A_{SLR}}{X_{I,\odot}M_\odot/A_I}\exp\left(-\Delta/\tau_{SLR}\right), \quad (5)$$

where τ_{SLR} is the decay timescale of the radioactive isotope and we use $\tau_{SLR} = 2.003\,$Myr [9] for ^{10}Be. $X_{I,\odot} = 1.4\times10^{-10}$[58] is the solar mass fraction of the stable reference isotope, ^{9}Be, with mass number A_I. There are two free parameters: f is the dilution factor (i.e. fraction of the CCSN ejecta incorporated into the proto-solar cloud) and Δ is the interval between the production of the SLR by the CCSN and its incorporation into ESS solids. We take a dilution factor of $f = 5\times10^{-4}$ and $\Delta = 1$ Myr, which allows us to match the measured ESS ratios of ^{41}Ca/^{40}Ca and ^{107}Pd/^{108}Pd for the 11.8 $M_\odot$ model, which is also consistent with constraints from CCSN remnant evolution models and the requirements for the injection of material from the shock into the proto-solar cloud [17]. Note that neither ^{41}Ca nor ^{107}Pd are significantly affected by the neutrino spectra or the reaction rates discussed here. With these parameters, the observed ^{10}Be/^{9}Be ESS ratio, $(3-9)\times10^{-4}$

[59] requires yields in the range $(1.5-4.6)\times10^{-10}\,M_\odot$.

In order to fully cover the range of uncertainties of the neutrino spectra we calculate the ^{10}Be yield for five different models. We took different assumptions about the neutrino spectra, including low E_ν (Model-1), the spectra from the simulation [31] (Model-2), and high E_ν (Model-3). We also include estimates for the maximum impact of neutrino flavor transformations by assuming a complete swap of the spectra of $\bar{\nu}_e$ and $\bar{\nu}_x$ for neutrino spectra from simulation (Model-4) as well as for high E_ν (Model-5). Table III shows the yields of the 11.8 $M_\odot$ model for the lower and recommended ^{10}Be$(p,\alpha)^7$Li reaction rate and different neutrino spectra models. These yield values are also shown in Figure 8, together with band representing the required ^{10}Be yields to match the inferred ^{10}Be/^{9}Be ratio. For both values of the ^{10}Be$(p,\alpha)^7$Li reaction rate, the highest ^{10}Be yields result from the high E_ν case with flavor transformations (Model-5), whereas the lowest yields result from the low E_ν case (Model-1). This shows that all the models, even with the most optimistic neutrino spectra and the lower ^{10}Be$(p,\alpha)^7$Li reaction rate, fall short of the required ^{10}Be yield in this scenario.

Here, we have not considered the uncertainties of the parameters f and Δ. Due to the very short half-life of ^{41}Ca, Δ is relatively well constrained while the dilution factor, f, is sensitive to the uncertainty of the ^{107}Pd/^{108}Pd ratio in the ESS, when we follow the argument of Banerjee *et al.* [17]. From this, we expect an uncertainty of up to a factor two for the required ^{10}Be yield. Taking this uncertainty into account, Fig. 8 shows that only Model-5, assuming maximal neutrino flavor transformations and with our lower rate for ^{10}Be$(p,\alpha)^7$Li can produce enough ^{10}Be to be in agreement with the observational constraints for this model.

A lower explosion energy could further increase the ^{10}Be yield. However, for the 11.8 $M_\odot$ model we already assume a low explosion energy of 0.3 $\times 10^{51}$ erg based on the 3D simulation which makes a significant increase unlikely. Furthermore, the uncertainties of stellar evolution calculations may allow models of similar mass with C-rich layers to be closer to the core and thus subject to a stronger neutrino flux, enhancing the ^{10}Be yield. The analysis of the impact of the details of stellar evolution on the yields, however, is beyond the scope of this article.

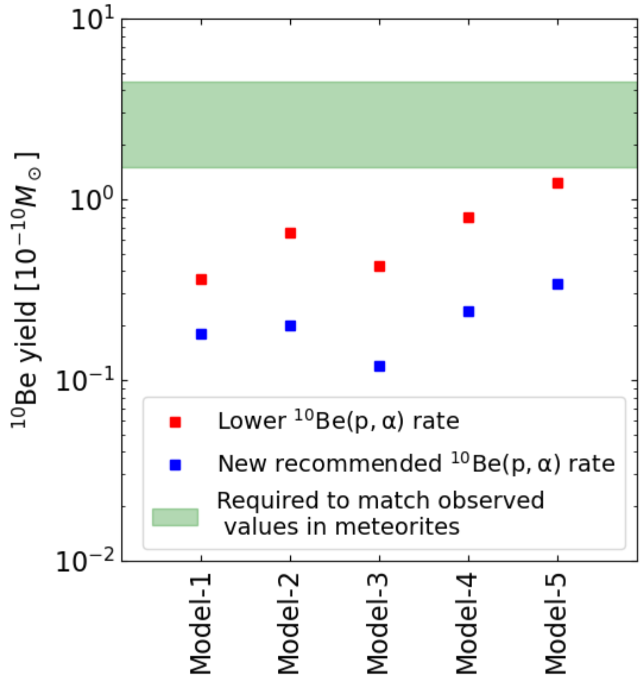

FIG. 8. ^{10}Be yield for the different models of the neutrino spectra listed in table III for the recommended and lower ^{10}Be$(p,\alpha)^7$Li reaction rate. The green band indicates the yield that is required to be in agreement with the observed ESS ^{10}Be/^{9}Be ratio when assuming the scenario of [17].

VI. CONCLUSIONS

We have studied the production of ^{10}Be by the ν process in CCSN explosions for a range of progenitors and for different models of the neutrino spectra, to investigate the role of the ^{10}Be$(p,\alpha)^7$Li, ^{10}Be$(\alpha,n)^{13}$C and ^{10}Be$(\nu_e,e^-)^{10}$B reactions as ^{10}Be destruction channels. An enhanced ^{10}Be$(p,\alpha)^7$Li reaction rate significantly reduces the yields of this SLR and it changes the relationship between the neutrino spectra and the net ^{10}Be yield. The large uncertainty of the ^{10}Be$(\alpha,n)^{13}$C reaction rate can change the ^{10}Be yield by a factor of 2, making it the second most important reaction, after the ^{10}Be$(p,\alpha)^7$Li reaction, as a destruction channel for ^{10}Be in CCSNe.

We re-evaluated the ^{10}Be$(p,\alpha)^7$Li reaction rate using R-matrix calculations based on updated nuclear data including the recently observed low energy resonance at 193 keV in the compound nucleus ^{11}B [44]. We show that this resonance makes the ^{10}Be$(p,\alpha)^7$Li reaction rate significantly larger (up to a factor of 20) than the rate in the JINA-REACLIB database. With our recommended rate, the ^{10}Be yields are up to a factor of 33 lower than those obtained with the default REACLIB rate. However, further experimental constraints on the proton and alpha widths of the 193 keV resonance are necessary to narrow down the range of calculated ^{10}Be yields. We show that, with the recommended ^{10}Be$(p,\alpha)^7$Li reaction rate, this 11.8 $M_\odot$ model cannot explain the ^{10}Be/^{9}Be ratio in agreement with other isotopic ratios inferred from meteorites, even with the most energetic neutrino spectra. With the lower ^{10}Be$(p,\alpha)^7$Li reaction rate, maximal flavor transformation are required to get close enough to the observed value to be in agreement if other uncertainties, such as the dilution factor and delay time in Eq. (5), are taken into account. Recent experimental results [51], however, exclude the lower ^{10}Be$(p,\alpha)^7$Li rate. Unless there are major changes in the models for the structure of stars in this mass range, these findings point towards a need for another source of ^{10}Be in the ESS, such as non-thermal, in-situ production. We encourage the further refinement in the prediction of CCSN neutrino spectra (including flavor transformations), stellar structure calculations, as well as experiments to constrain the properties of 193 keVresonance in the $^{10}\mathrm{Be}(p,\alpha)^{7}\mathrm{Li}$ reaction and the $^{10}\mathrm{Be}(\alpha,n)^{13}\mathrm{C}$ reaction rate to further constrain our findings.

ACKNOWLEDGMENTS

This work was supported by the U.S. Department of Energy, Office of Science, Office of Nuclear Physics and Office of Advanced Scientific Computing Research, Scientific Discovery through Advanced Computing (SciDAC) program. Research at Oak Ridge National Laboratory is supported under contract DE-AC05-00OR22725 from the U.S. Department of Energy to UT-Battelle, LLC. JSR, RJD and TA were supported by National Science Foundation through Grant No. Phys-2011890. RJD utilized resources from the Notre Dame Center for Research Computing and was supported by the Joint Institute for Nuclear Astrophysics through Grant No. PHY-1430152 (JINA Center for the Evolution of the Elements). RM and GMP acknowledge the support of the Deutsche Forschungsgemeinschaft (DFG, German Research Foundation) – Project-ID 279384907 – SFB 1245 "Nuclei: From Fundamental Interactions to Structure and Stars". This research made extensive use of numpy [60], matplotlib [61] and of the SAO/NASA Astrophysics Data System (ADS).

Appendix A: $^{10}\mathrm{Be}(p,\alpha)^{7}\mathrm{Li}$ rate: REACLIB fit parameters

In the REACLIB reaction rate library, thermonuclear reaction rates are described as a function of temperature in GK, T, by a seven parameter fit as

$$\langle\sigma v\rangle(T) = \exp\left[a_0 + \left(\sum_{i=1}^{5} a_i\, T^{\frac{2i-5}{3}}\right) + a_6 \ln(\mathrm{T})\right]. \quad \text{(A1)}$$

Resonant and non-resonant contributions need to be fitted by separate sets of parameters. Table IV gives the fit parameters for the lower and recommended rate for the $^{10}\mathrm{Be}(p,\alpha)^{7}\mathrm{Li}$ reaction discussed in IV. Each fit consists of two sets of seven parameters, for the resonant and non-resonant contributions. The fit is illustrated for the recommended rate in Fig. 9. Deviations of the fit from the R-matrix calculation are less than 5 % for temperatures higher than 0.3 GK. The parameters for the reverse reaction rate can be obtained from the forward reaction by detailed balance by replacing $a_0^{\mathrm{rev}} = a_0 - 2.2375$ and $a_1^{\mathrm{rev}} = a_1 - 29.7539$. The other parameters $a_{2\ldots6}$ remain the same [62].

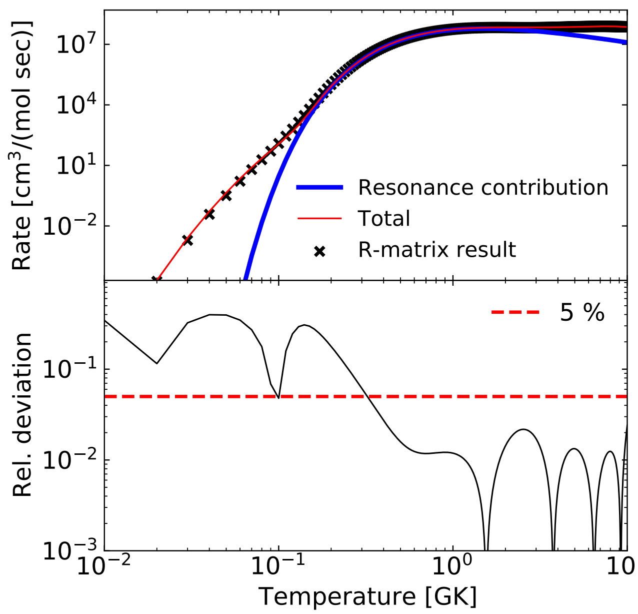

FIG. 9. Reaction rate fit with the REACLIB parameterization, using a resonant and non-resonant contribution. The parameterization and reaction rate calculation agree within 5 % for all temperatures above 0.3 GK, which are the most relevant for CCSN explosions.

TABLE IV. Fit parameters for the lower and recommended rate. Each rate consists of a resonant and non-resonant contribution.

	lower		Recommended	
	resonant	non-resonant	resonant	non-resonant
a_0	18.83813	30.49055	20.01675	29.05572
a_1	-2.236187	0.0	-2.236187	0.0
a_2	0.0	-11.32177	0.0	-11.25624
a_3	0.0	-9.265300	0.0	-3.687460
a_4	0.0	3.559158	0.0	0.7607396
a_5	0.0	-0.5154761	0.0	0.08781213
a_6	-1.5	-2/3	-1.5	-2/3

[1] T. Lee, D. A. Papanastassiou, and G. J. Wasserburg, Aluminum-26 in the early solar system: fossil or fuel?, Astrophys. J. Lett. **211**, L107 (1977).

[2] J. H. Reynolds, Determination of the Age of the Elements, Phys. Rev. Lett. **4**, 8 (1960).

[3] N. Dauphas and M. Chaussidon, A Perspective from Ex-

tinct Radionuclides on a Young Stellar Object: The Sun and Its Accretion Disk, Annu. Rev. of Earth and Planet. Sci. **39**, 351 (2011).

[4] M. Lugaro, U. Ott, and Á. Kereszturi, Radioactive nuclei from cosmochronology to habitability, Prog. Part. Nucl. Phys. **102**, 1 (2018).

[5] C. Zucker, A. A. Goodman, J. Alves, S. Bialy, M. Foley, J. S. Speagle, J. Großschedl, D. P. Finkbeiner, A. Burkert, D. Khimey, and C. Swiggum, Star formation near the Sun is driven by expansion of the Local Bubble, Nature **601**, 334 (2022).

[6] J. C. Forbes, J. Alves, and D. N. C. Lin, A Solar System formation analogue in the Ophiuchus star-forming complex, Nature Astronomy **5**, 1009 (2021).

[7] M. G. H. Krause, A. Burkert, R. Diehl, K. Fierlinger, B. Gaczkowski, D. Kroell, J. Ngoumou, V. Roccatagliata, T. Siegert, and T. Preibisch, Surround and Squash: the impact of superbubbles on the interstellar medium in Scorpius-Centaurus OB2, Astron. Astrophys. **619**, A120 (2018).

[8] A. Cameron and J. Truran, The supernova trigger for formation of the solar system, Icarus **30**, 447 (1977).

[9] J. Chmeleff, F. von Blanckenburg, K. Kossert, and D. Jakob, Determination of the ^{10}Be half-life by multicollector ICP-MS and liquid scintillation counting, Nuclear Instruments and Methods in Physics Research B **268**, 192 (2010).

[10] K. Fukuda, H. Hiyagon, W. Fujiya, N. Takahata, T. Kagoshima, and Y. Sano, Origin of the Short-lived Radionuclide ^{10}Be and Its Implications for the Astronomical Setting of CAI Formation in the Solar Protoplanetary Disk, Astrophys. J. **886**, 34 (2019).

[11] V. Tatischeff, J. Duprat, and N. de Séréville, Light-element Nucleosynthesis in a Molecular Cloud Interacting with a Supernova Remnant and the Origin of Beryllium-10 in the Protosolar Nebula, Astrophys. J. **796**, 124 (2014).

[12] J. Duprat and V. Tatischeff, Energetic Constraints on In Situ Production of Short-Lived Radionuclei in the Early Solar System, Astrophys. J. Lett. **671**, L69 (2007).

[13] S. J. Desch, J. Connolly, Harold C., and G. Srinivasan, An Interstellar Origin for the Beryllium 10 in Calcium-rich, Aluminum-rich Inclusions, Astrophys. J. **602**, 528 (2004).

[14] T. Lee, F. H. Shu, H. Shang, A. E. Glassgold, and K. E. Rehm, Protostellar Cosmic Rays and Extinct Radioactivities in Meteorites, Astrophys. J. **506**, 898 (1998).

[15] S. E. Woosley, D. H. Hartmann, R. D. Hoffman, and W. C. Haxton, The ν-process, Astrophys. J. **356**, 272 (1990).

[16] K. G. Balasi, K. Langanke, and G. Martínez-Pinedo, Neutrino-nucleus reactions and their role for supernova dynamics and nucleosynthesis, Progress in Particle and Nuclear Physics **85**, 33 (2015).

[17] P. Banerjee, Y.-Z. Qian, A. Heger, and W. C. Haxton, Evidence from stable isotopes and ^{10}Be for solar system formation triggered by a low-mass supernova, Nature Commun. **7**, 13639 (2016).

[18] H. Tang and N. Dauphas, Low ^{60}Fe Abundance in Semarkona and Sahara 99555, Astrophys. J. **802**, 22 (2015).

[19] H. Tang and N. Dauphas, Abundance, distribution, and origin of ^{60}Fe in the solar protoplanetary disk, Earth and Planet. Sci. Lett. **359**, 248 (2012).

[20] R. H. Cyburt, A. M. Amthor, R. Ferguson, Z. Meisel, K. Smith, S. Warren, A. Heger, R. D. Hoffman, T. Rauscher, A. Sakharuk, H. Schatz, F. K. Thielemann, and M. Wiescher, The JINA REACLIB Database: Its Recent Updates and Impact on Type-I X-ray Bursts, Astrophys. J. Suppl. Ser. **189**, 240 (2010).

[21] `https://reaclib.jinaweb.org/index.php`.

[22] R. V. Wagoner, Synthesis of the Elements Within Objects Exploding from Very High Temperatures, Astrophys. J. Suppl. Ser. **18**, 247 (1969).

[23] A. Sieverding, B. Müller, and Y. Z. Qian, Nucleosynthesis of an 11.8 $M_\odot$ Supernova with 3D Simulation of the Inner Ejecta: Overall Yields and Implications for Short-lived Radionuclides in the Early Solar System, Astrophys. J. **904**, 163 (2020).

[24] A. Sieverding, G. Martínez-Pinedo, L. Huther, K. Langanke, and A. Heger, The ν-Process in the Light of an Improved Understanding of Supernova Neutrino Spectra, Astrophys. J. **865**, 143 (2018).

[25] K. Lodders, Solar System Abundances and Condensation Temperatures of the Elements, Astrophys. J. **591**, 1220 (2003).

[26] S. E. Woosley, A. Heger, and T. A. Weaver, The evolution and explosion of massive stars, Rev. Mod. Phys. **74**, 1015 (2002).

[27] T. A. Weaver, G. B. Zimmerman, and S. E. Woosley, Presupernova evolution of massive stars., Astrophys. J. **225**, 1021 (1978).

[28] R. Bollig, N. Yadav, D. Kresse, H.-T. Janka, B. Müller, and A. Heger, Self-consistent 3D Supernova Models From -7 Minutes to +7 s: A 1-bethe Explosion of a 19 $M_\odot$ Progenitor, Astrophys. J. **915**, 28 (2021).

[29] D. Vartanyan, A. Burrows, D. Radice, M. A. Skinner, and J. Dolence, A successful 3D core-collapse supernova explosion model, Mon. Not. R. Astron. Soc. **482**, 351 (2019).

[30] E. J. Lentz, S. W. Bruenn, W. R. Hix, A. Mezzacappa, O. E. B. Messer, E. Endeve, J. M. Blondin, J. A. Harris, P. Marronetti, and K. N. Yakunin, Three-dimensional Core-collapse Supernova Simulated Using a 15 $M_\odot$ Progenitor, Astrophys. J. Lett. **807**, L31 (2015).

[31] B. Müller, T. M. Tauris, A. Heger, P. Banerjee, Y.-Z. Qian, J. Powell, C. Chan, D. W. Gay, and N. Langer, Three-dimensional simulations of neutrino-driven core-collapse supernovae from low-mass single and binary star progenitors, Mon. Not. R. Astron. Soc. **484**, 3307 (2019).

[32] `https://github.com/starkiller-astro/XNet`.

[33] T. Yoshida, T. Suzuki, S. Chiba, T. Kajino, H. Yokomakura, K. Kimura, A. Takamura, and D. H. Hartmann, Neutrino-Nucleus Reaction Cross Sections for Light Element Synthesis in Supernova Explosions, Astrophys. J. **686**, 448 (2008).

[34] M. Kusakabe, M.-K. Cheoun, K. S. Kim, M.-a. Hashimoto, M. Ono, K. Nomoto, T. Suzuki, T. Kajino, and G. J. Mathews, Supernova Neutrino Process of Li and B Revisited, Astrophys. J. **872**, 164 (2019).

[35] M.-R. Wu, Y.-Z. Qian, G. Martínez-Pinedo, T. Fischer, and L. Huther, Effects of neutrino oscillations on nucleosynthesis and neutrino signals for an $18 M_\odot$ supernova model, Phys. Rev. C **91**, 065016 (2015).

[36] T. Yoshida, T. Kajino, H. Yokomakura, K. Kimura, A. Takamura, and D. H. Hartmann, Supernova Neutrino Nucleosynthesis of Light Elements with Neutrino Oscillations, Phys. Rev. Lett. **96**, 091101 (2006).

[37] N. V. Eremin, S. S. Zeinalov, A. P. Kabachenko, D. V. Kamanin, K. D. Medina, V. F. Strizhov, and G. M. Ter-Akopyan, Investigation of resonance structures in 10 b(p, n) reaction at low proton energies, in *Proc.37th Ann.Conf.Nucl.Spectrosc.Struct.At.Nuclei, Yurmala* (1987) p. 300.

[38] A. Sieverding, K. Langanke, G. Martínez-Pinedo, R. Bollig, H. T. Janka, and A. Heger, The ν-process with Fully Time-dependent Supernova Neutrino Emission Spectra, Astrophys. J. **876**, 151 (2019), arXiv:1902.06643 [astro-ph.HE].

[39] A. L. Sallaska, C. Iliadis, A. E. Champange, S. Goriely, S. Starrfield, and F. X. Timmes, STARLIB: A Next-generation Reaction-rate Library for Nuclear Astrophysics, Astrophys. J. Suppl. Ser. **207**, 18 (2013).

[40] D. R. Tilley, J. H. Kelley, J. L. Godwin, D. J. Millener, J. E. Purcell, C. G. Sheu, and H. R. Weller, Energy levels of light nuclei $A = 8$, 9, 10, Nucl. Phys. A **745**, 155 (2004).

[41] E. Caurier, G. Martínez-Pinedo, F. Nowacki, A. Poves, and A. P. Zuker, The shell model as unified view of nuclear structure, Rev. Mod. Phys. **77**, 427 (2005).

[42] S. Cohen and D. Kurath, Effective interactions for the 1p shell, Nucl. Phys. **73**, 1 (1965).

[43] W.-T. Chou, E. K. Warburton, and B. A. Brown, Gamow-Teller beta-decay rates for $A \leq 18$ nuclei, Phys. Rev. C **47**, 163 (1993).

[44] Y. Ayyad, B. Olaizola, W. Mittig, G. Potel, V. Zelevinsky, M. Horoi, S. Beceiro-Novo, M. Alcorta, C. Andreoiu, T. Ahn, M. Anholm, L. Atar, A. Babu, D. Bazin, N. Bernier, S. S. Bhattacharjee, M. Bowry, R. Caballero-Folch, M. Cortesi, C. Dalitz, E. Dunling, A. B. Garnsworthy, M. Holl, B. Kootte, K. G. Leach, J. S. Randhawa, Y. Saito, C. Santamaria, P. Šiurytė, C. E. Svensson, R. Umashankar, N. Watwood, and D. Yates, Direct observation of proton emission in ^{11}Be, Phys. Rev. Lett. **123**, 082501 (2019).

[45] J. Okołowicz, M. Płoszajczak, and W. Nazarewicz, Convenient location of a near-threshold proton-emitting resonance in ^{11}B, Phys. Rev. Lett. **124**, 042502 (2020).

[46] R. E. Azuma, E. Uberseder, E. C. Simpson, C. R. Brune, H. Costantini, R. J. de Boer, J. Görres, M. Heil, P. J. LeBlanc, C. Ugalde, and M. Wiescher, AZURE: An R-matrix code for nuclear astrophysics, Phys. Rev. C **81**, 045805 (2010).

[47] E. Uberseder and R. J. deBoer, *AZURE2 User Manual* (2015), azure.nd.edu.

[48] J. Refsgaard, J. Büscher, A. Arokiaraj, H. O. U. Fynbo, R. Raabe, and K. Riisager, Clarification of large-strength transitions in the β decay of ^{11}Be, Phys. Rev. C **99**, 044316 (2019).

[49] https://www.nndc.bnl.gov/nudat3/getdataset.jsp?nucleus=11B&unc=NDS.

[50] C. Angulo, M. Arnould, M. Rayet, P. Descouvemont, D. Baye, C. Leclercq-Willain, A. Coc, S. Barhoumi, P. Aguer, C. Rolfs, R. Kunz, J. Hammer, A. Mayer, T. Paradellis, S. Kossionides, C. Chronidou, K. Spyrou, S. Degl'Innocenti, G. Fiorentini, B. Ricci, S. Zavatarelli, C. Providencia, H. Wolters, J. Soares, C. Grama, J. Rahighi, A. Shotter, and M. Lamehi Rachti, A compilation of charged-particle induced thermonuclear reaction rates, Nucl. Phys. A **656**, 3 (1999).

[51] Y. Ayyad, W. Mittig, T. Tang, B. Olaizola, G. Potel, N. Rijal, N. Watwood, H. Alvarez-Pol, D. Bazin, M. Caamaño, J. Chen, M. Cortesi, B. Fernández-Domínguez, S. Giraud, P. Gueye, S. Heinitz, R. Jain, B. P. Kay, E. A. Maugeri, B. Monteagudo, F. Ndayisabye, S. N. Paneru, J. Pereira, E. Rubino, C. Santamaria, D. Schumann, J. Surbrook, L. Wagner, J. C. Zamora, and V. Zelevinsky, Evidence of a near-threshold resonance in ^{11}B relevant to the β-delayed proton emission of ^{11}Be, arXiv e-prints , arXiv:2205.04973 (2022), arXiv:2205.04973 [nucl-ex].

[52] S. Almaraz-Calderon, In prep. (2022).

[53] K. Ebinger, S. Curtis, C. Fröhlich, M. Hempel, A. Perego, M. Liebendörfer, and F.-K. Thielemann, PUSHing Core-collapse Supernovae to Explosions in Spherical Symmetry. II. Explodability and Remnant Properties, Astrophys. J. **870**, 1 (2019).

[54] M. Hamuy, Observed and Physical Properties of Core-Collapse Supernovae, Astrophys. J. **582**, 905 (2003), arXiv:astro-ph/0209174 [astro-ph].

[55] O. Pejcha and J. L. Prieto, On the Intrinsic Diversity of Type II-Plateau Supernovae, Astrophys. J. **806**, 225 (2015), arXiv:1501.06573 [astro-ph.SR].

[56] T. Müller, J. L. Prieto, O. Pejcha, and A. Clocchiatti, The Nickel Mass Distribution of Normal Type II Supernovae, Astrophys. J. **841**, 127 (2017), arXiv:1702.00416 [astro-ph.SR].

[57] G. J. Wasserburg, M. Busso, R. Gallino, and K. M. Nollett, Short-lived nuclei in the early Solar System: Possible AGB sources, Nucl. Phys. A **777**, 5 (2006).

[58] M. Asplund, N. Grevesse, A. J. Sauval, and P. Scott, The Chemical Composition of the Sun, Annu. Rev. Astron. Astrophys. **47**, 481 (2009).

[59] M.-C. Liu, M. Chaussidon, G. Srinivasan, and K. D. McKeegan, A Lower Initial Abundance of Short-lived ^{41}Ca in the Early Solar System and Its Implications for Solar System Formation, Astrophys. J. **761**, 137 (2012).

[60] S. van der Walt, S. C. Colbert, and G. Varoquaux, The numpy array: A structure for efficient numerical computation, Computing in Science Engineering **13**, 22 (2011).

[61] J. D. Hunter, Matplotlib: A 2D Graphics Environment, Computing in Science and Engineering **9**, 90 (2007).

[62] T. Rauscher and F.-K. Thielemann, Astrophysical Reaction Rates From Statistical Model Calculations, At. Data Nucl. Data Tables **75**, 1 (2000).